

# Sensitivity of coherent range-resolved differential absorption lidar

Takayasu Fukuda, Yoshio Matsuura, and Tadatami Mori

A range-resolved DIAL (differential absorption lidar) system with heterodyne detection has been developed. A hybrid TEA CO<sub>2</sub> laser was employed as the transmitter oscillator, which emitted single-frequency pulses of 140 mJ. The heterodyne receiver, which had a minimum detectable power of  $2 \times 10^{-11}$  W, could detect the echo signals backscattered from atmospheric aerosols at a 5-km or greater range. The system sensitivity to the target gas, defined as the product of the minimum detectable concentration and the difference in the absorption coefficients, was experimentally found to be  $3.7 \times 10^{-4}$  m<sup>-1</sup> for a range resolution of 300 m after averaging over fifty backscattered signals.

## I. Introduction

The range-resolved differential absorption (RRDA) lidar technique offers an alternative to *in situ* sensors for the measurement of gaseous constituents in the atmosphere. RRDA lidar systems use a pulsed laser transmitter with atmospheric aerosol particles as the backscattering medium to perform the range-resolved measurements. Because of its range resolution, this technique has been attracting much attention and recently systems with different types of laser have been reported.<sup>1-3</sup>

Among these, the RRDA lidar with CO<sub>2</sub> laser has advantages in weather penetration capability and versatility; in the wavelength region of lasing transition of CO<sub>2</sub> there are absorption lines from a number of gas species, O<sub>3</sub>, H<sub>2</sub>O, NH<sub>3</sub>, and so forth. In spite of these advantages, few such systems have been reported, because the scattering cross section of aerosols is extremely small and a direct-detection system would require a transmitter oscillator of high energy, several joules, for example.<sup>3</sup> In this wavelength region, however, sensitivity with heterodyne (coherent) detection can be made much higher than with direct detection. Kobayasi and Inaba<sup>4</sup> proposed the RRDA lidar with heterodyne detection, which has high range performance with a low

energy laser. Although their proposal seemed promising, technical difficulties have prevented its realization so far.

As the minimum detectable power (MDP) of a heterodyne receiver is proportional to the IF bandwidth, the optical bandwidth of the transmitted laser pulse must be narrow and its center frequency must be stable. Because of a wide (~1-GHz) bandwidth, the conventional TEA CO<sub>2</sub> laser, with all its high energy output, is not suitable for use as the transmitter oscillator of a coherent lidar. Even if we could obtain a highly coherent transmitter, the narrow bandwidth of its output pulse, which is comparable with that of the receiver, would cause another problem: return signal fluctuation,<sup>5</sup> which is referred to as speckle noise. Since the accuracy of the gas concentration inferred from RRDA measurements is impaired by errors in determining the amplitude of the signal, speckle fluctuation, dominating the errors in the large signal limit,<sup>6</sup> should be suppressed to improve the system sensitivity to the target gas.

We have developed a coherent RRDA lidar which deals with these problems. A hybrid TEA CO<sub>2</sub> laser was employed as the highly coherent transmitter. Among the various mode-selection methods, we chose to use the hybrid approach because it is reliable and because it provides a continuous reference laser output for adjusting the output pulse frequency. To reduce the speckle fluctuation in return signals, we incorporated interpulse averaging of signals.

In this paper we shall describe an experimental study of the achieved performance of a newly developed coherent DIAL which includes range capability, heterodyne efficiency, and detection sensitivity to the target gas. This seems to be the first work which has given an experimental basis to a sensitivity analysis of coherent RRDA lidar.<sup>6,7</sup>

The authors are with Fujitsu System Integration Laboratories, Ltd., Electronics System Department, 1333, Kamikodanaka, Nakahara-ku, Kawasaki 211, Japan.

Received 12 November 1983.

0003-6935/84/122026-07\$02.00/0.

© 1984 Optical Society of America.

## II. Detection Sensitivity of Coherent RRDA Lidar

In the RRDA technique, echo signal measurements are made at two wavelengths  $\lambda_0$  and  $\lambda_1$ , respectively, off and on the absorption resonance of the target gas. The gas concentration  $C(R)$  at range  $R$  is deduced from the measured received power using the following equation:

$$C(R) = \frac{1}{2\Delta k \Delta R} \ln \left[ \frac{\langle P_r^1(R - \Delta R/2) \rangle \langle P_r^0(R + \Delta R/2) \rangle}{\langle P_r^1(R + \Delta R/2) \rangle \langle P_r^0(R - \Delta R/2) \rangle} \right],$$

where  $\Delta k$  = difference in absorption coefficient between the two wavelengths,

$\Delta R$  = range interval, and

$\langle P_r^0 \rangle, \langle P_r^1 \rangle$  = expected value of the received power for wavelengths  $\lambda_0$  and  $\lambda_1$ .

The concentration uncertainty  $\sigma_c^2$  is given as<sup>7</sup>

$$\sigma_c^2 = \frac{1}{4(\Delta k)^2(\Delta R)^2} \left\{ \frac{\text{var}[P_r^0(R + \Delta R/2)]}{\langle P_r^0(R + \Delta R/2) \rangle^2} + \frac{\text{var}[P_r^0(R - \Delta R/2)]}{\langle P_r^0(R - \Delta R/2) \rangle^2} + \frac{\text{var}[P_r^1(R + \Delta R/2)]}{\langle P_r^1(R + \Delta R/2) \rangle^2} + \frac{\text{var}[P_r^1(R - \Delta R/2)]}{\langle P_r^1(R - \Delta R/2) \rangle^2} \right\}, \quad (1)$$

where we assumed that samples of  $P_r$  are not correlated with each other.<sup>8</sup> Granted that the range dependence of  $P_r$  is not significant, Eq. (1) can be reduced to

$$\sigma_c^2 = \frac{1}{(\Delta k)^2(\Delta R)^2} \left[ \frac{\text{var}(P_r)}{\langle P_r \rangle^2} \right]. \quad (2)$$

In Eq. (2), the ratio  $\langle P_r \rangle / [\text{var}(P_r)]^{1/2}$  is a measure of the relative amplitude accuracy. We refer to this ratio as inverse relative root variance of the measured received power [IRRV( $P_r$ )] in accordance with Jakeman *et al.*<sup>5</sup>

For a coherent lidar, IRRV of the IF output, IRRV( $P_{IF}$ ), is given as<sup>9</sup>

$$\text{IRRV}(P_{IF}) = \left[ \frac{\text{CNR}/2}{1 + \text{CNR}/2\text{IRRV}_0^2 + (2\text{CNR})^{-1}} \right]^{1/2}, \quad (3)$$

where the carrier-to-noise ratio (CNR),

$$\text{CNR} = \langle P_r \rangle / \text{MDP}, \quad (4)$$

is the ratio of the mean signal and mean noise contributions of IF output, and IRRV<sub>0</sub> is the IRRV of the signal component. In the large signal limit (CNR > 5), Eq. (3) is reduced to IRRV( $P_{IF}$ )  $\approx$  IRRV<sub>0</sub>, and speckle fluctuation dominates IRRV<sub>0</sub>, which is  $\sqrt{M}$  if the receiver views  $M$  coherent areas. Because the video signal extracted from the IF output is smoothed by the video amplifier, IRRV( $P_r$ ) for the single-pulse echo, IRRV<sub>1</sub>, is given as

$$\text{IRRV}_1 = \sqrt{MB_I T}, \quad (5)$$

where  $B_I$  = intensity fluctuation bandwidth, and  $T$  = integration time of the video amplifier. If the echoes are not correlated with each other, by averaging their  $N$  video signals, IRRV( $P_r$ ) will be improved to

$$\text{IRRV}(P_r) = \sqrt{N} \text{IRRV}_1 = \sqrt{NMB_I T}. \quad (6)$$

Thus, the standard deviation of the deduced gas concentration is given as  $\sigma_c = 1/(\Delta k \Delta R \sqrt{NMB_I T})$ . Strictly speaking, the experimental estimation of  $\sigma_c$  should be done from samples of  $C(R)$  for a particular

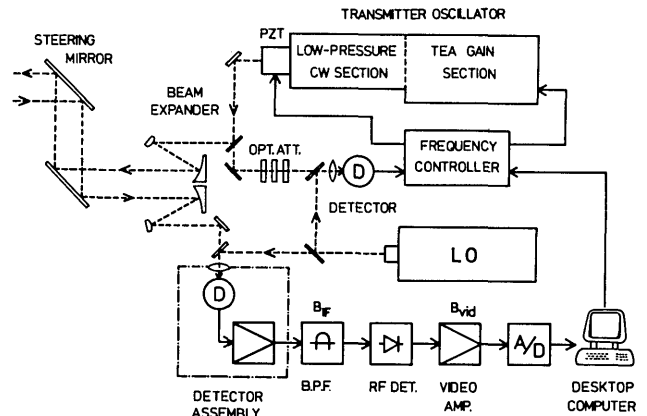


Fig. 1. RRDA lidar with heterodyne detection.

range. Since it would take a long time to derive  $\sigma_c$  with accuracy in this manner, we calculated it from the samples of  $C$  in one distribution profile, assuming that IRRV was independent of range.

The value  $\Delta k \sigma_c$  is an estimate of the measurement accuracy which is independent of the target gas species. We will refer to this as the system sensitivity  $S$ , that is,

$$S \equiv \Delta k \sigma_c = 1/(\Delta R \sqrt{MNB_I T}). \quad (7)$$

Similarly we will define the generalized gas concentration  $C_0$  as  $\Delta k C$ . The dimension of these quantities, by definition, is ( $\text{m}^{-1}$ ).

In a heterodyne receiver, MDP in Eq. (4) is given as

$$\text{MDP} = \frac{h\nu B_{IF}}{\eta_D \eta_{\text{sys}}}, \quad (8)$$

where  $h\nu$  = photon energy,

$B_{IF}$  = IF bandwidth,

$\eta_D$  = heterodyne equivalent quantum efficiency of the detector, and

$\eta_{\text{sys}}$  = efficiency of the receiver optics.

The antenna efficiency in heterodyne reception of incoherent backscatter signals is incorporated in  $\eta_{\text{sys}}$ .

## III. System Description

A block diagram of the experimental coherent DIAL system is shown in Fig. 1. The system consisted of the transmitter oscillator, detectors, local oscillator (LO), desktop computer, transmitter frequency controller, and transmitting and receiving antennas.

The transmitter oscillator was a hybrid TEA CO<sub>2</sub> laser consisting of a TEA gain section and a low-pressure gain section in a common optical cavity formed from a Littrow mounted concave grating and a flat output coupler. The output coupler was mounted on a piezoelectric translator. The transmitter oscillator produced a single-frequency output with a cw output power of  $\sim 1$  W and a pulsed output energy of 140 mJ/pulse at 5 pps.

The detectors, one for the receiver and the other for the frequency controller, were wide-bandwidth HgCdTe

Table I. Lidar Parameters

Transmitter (hybrid TEA CO <sub>2</sub> laser)	
Pulse energy ( $E_t$ )	140 mJ [10.6- $\mu$ m P(24)]
Pulse duration ( $\tau_p$ )	250 nsec
Repetition rate (PRF)	5–20 Hz
cw output power ( $P_{cw}$ )	1 W
Detector (HgCdTe photodiode)	
Responsivity	5.5 A/W
Quantum efficiency	0.64
Heterodyne efficiency ( $\eta_D$ )	0.1–0.3
Transmitter/receiver telescope	
Aperture area ( $A_r$ )	177 cm <sup>2</sup> (15 cm $\phi$ )
Receiver electronics	
IF bandwidth ( $B_{IF}$ )	10 MHz
Video bandwidth ( $B_{vid}$ )	0.55/1.5 MHz
A–D sampling time	100 nsec
A–D resolution	8 bit

photodiodes<sup>10</sup> whose performance is shown in Table I. The received signal was mixed with LO output at the receiver photodiode, and the IF signal was fed to a preamplifier through a bias insertion unit. The photodiode and the preamplifier were assembled together in a shielded housing so that noise caused by the TEA gain section would not interfere with the low level IF signal.

The local oscillator was a conventional cw laser whose cooling water temperature was controlled to an accuracy of 0.2°C to stabilize the LO frequency. The LO output beam was expanded to ~1 cm in diameter, which was equal to the diameter of the receiving telescope exit pupil.

The IF signal regulated by a step attenuator was demodulated by the linear envelope detector to extract the video signal. The 8-bit A–D converter (transient recorder) sampled and digitized the video signal and stored it in its memory. The digitized samples of the return signal were transferred to the computer by direct memory access (DMA). The computer integrated the signals and processed them to display a backscattered signal waveform or a gas distribution profile on a CRT. The computer made a hard copy of the CRT display.

A portion of the transmitter cw output and the LO output was mixed at the other detector, and the resultant IF signals were fed to the frequency controller, where a frequency discriminator detected the deviation of the beat frequency from a set frequency (12 MHz), and the error signal was fed back to the piezoelectric translator on which the output coupler of the transmitter was mounted. The TEA gain section was triggered at the very moment when the fluctuating IF coincided with the set point. Although a rapid (~1-kHz) fluctuation of the cw output frequency was caused by mechanical vibration of the transmitter laser resonator, this triggering technique adequately reduced its effect on the pulse output frequency.

The transmitting and receiving antennas were two identical folded off-axis beam expanders, 15 cm in diameter, which expanded the output beam and condensed the collected echo signal beam by a factor of 15.

The field of view of the system could be steered by a mirror to aim at the target. The field of view of the receiver and the transmitted beam could be crossed at any range from ~100 m to infinity.

The pulse repetition rate, IF bandwidth, IF signal attenuation, sampling rate, and number of integrations could be set through the computer keyboard. Laser line selection of the transmitter and local oscillator was performed manually and took ~1 min.

## IV. Performance

### A. Transmitter Output

Figure 2(a) is a typical waveform of the transmitter output pulse with duration of ~250 nsec. The waveform was observed by a HgCdTe photodiode whose bandwidth was ~250 MHz, and seems to have no mode beating.

Figure 2(b) shows the output pulse frequency characteristics observed in an IF waveform of the return pulse from a hard target. The optical frequency of the output pulse was precisely controlled to the set point by the technique described above. Pulse-to-pulse deviation of the optical frequency was within ~0.5 MHz. No intrapulse chirp was found for 1  $\mu$ sec from a pulse buildup.

Neither beam profile nor beam divergence for pulse operation was measured, but they can be estimated from those obtained in cw operation. The beam profile of the cw laser output at the telescope aperture is shown in Fig. 3. The Gaussian-like beam profiles suggest that the transmitter laser oscillates on the lowest transverse resonator mode. Defining beam radius  $w_0$  as the distance at which the power is  $1/e^2$  times that on the axis,

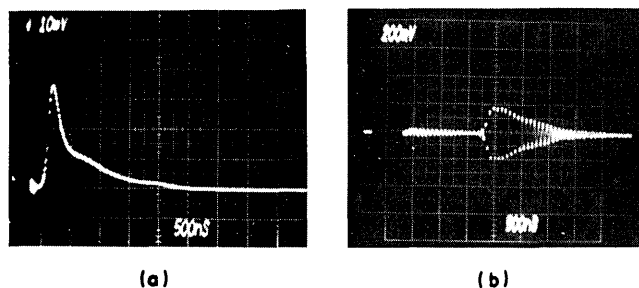


Fig. 2. Pulse shape and frequency characteristics: (a) transmitter output pulse, (b) received pulse at IF amplifier output.

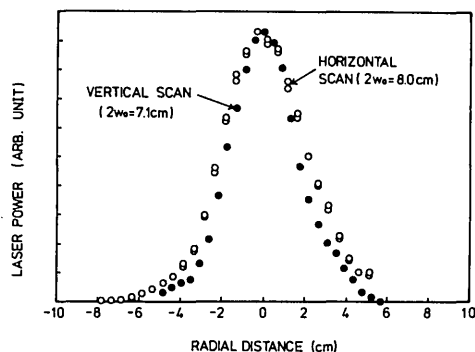


Fig. 3. Beam power profile of the cw output at the telescope aperture;  $w_0$  is  $1/e^2$  power radius.

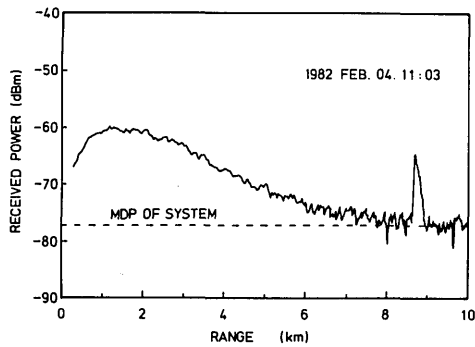


Fig. 4. Backscattered signal vs range;  $N = 50$ ,  $B_{\text{vid}} = 1.5$  MHz,  $\beta = 3 \times 10^{-8} \text{ m}^{-1} \text{ sr}^{-1}$ . The sharp peak is an echo signal from a hillside at  $\sim 9$  km.

the diameters or  $2w_0$  were estimated to be 8.0 and 7.1 cm from the horizontal and vertical scan profiles, respectively. The difference in  $w_0$  may be due to the aberration caused by the Littrow mounted concave grating. Beam divergence is estimated to be 0.19 mrad, assuming that the beam waist is at the aperture.

### B. System Efficiency Determination

The heterodyne receiver was calibrated to determine the system MDP. For this calibration, we used the cw output of the hybrid TEA laser, because the available CNR is moderate and optical attenuators, which would cause measurement errors, are not required. Targets were sandblasted aluminum plates, 50 cm in diameter, whose reflection coefficient  $\rho$  had been determined in advance of the field test. The reflected power  $P_r$  incident on the receiving aperture can be estimated using the following equation:

$$P_r = \frac{P_{\text{cw}} \rho A_r}{\pi R^2} \exp(-2\alpha R),$$

where  $P_{\text{cw}}$  = transmitted cw power,  
 $A_r$  = receiver aperture area,  
 $R$  = target range, and  
 $\alpha$  = extinction coefficient.

We evaluated  $\alpha$  from the relative humidity and the temperature at that time.<sup>11</sup> The received signals returned from the target were integrated for 100 sec and compared with the noise level to obtain the CNR. The system MDP and the overall efficiency  $\eta_D \eta_{\text{sys}}$  were determined from the estimated  $P_r$  and measured CNR. For  $B_{\text{IF}} = 10$  MHz, MDP was determined to be  $1.0$ – $2.0 \times 10^{-11}$  W. The value varied depending on the heterodyne efficiency of the detector employed or  $\eta_D$ . The lowest value,  $1.0 \times 10^{-11}$  W for  $\eta_D = 0.3$ , corresponds to  $\eta_{\text{sys}} = 0.063$ . We calibrated the receiver time after time to correct the system MDP value which was used to derive  $P_r$  from the CNR. The scatter in the measured MDP values was 10% at the most.

We measured IRRV of the signal returned from the target at the 430-nm range to estimate the spatial averaging factor  $M$ . In this case, the fluctuation bandwidth was  $<1$  kHz, and the postdetection integration had no effect. So, it follows that  $\text{IRRV}_1 = \sqrt{M}$ . From measured IRRV values, which ranged from 0.80 to 1.05, we concluded that  $M$  was unity and that the effect of

spatial averaging was negligible at any range greater than  $\sim 500$  m. This conclusion also means that there is no need to take account of the range dependence of the antenna efficiency in heterodyne reception of incoherent backscattered signals.

### C. Aerosol Backscatter Measurement and Available CNR

A waveform of the averaged echo returned from atmospheric aerosols is shown in Fig. 4. To obtain this waveform, fifty echoes were integrated. The dashed line is the MDP of the system as determined by the calibration described above. The sharp peak was an echo signal returned from a hillside  $\sim 9$  km from the lidar.

Such experiments were repeated at all seasons to determine the maximum useful range of the lidar. When  $\alpha$  was not extremely high ( $\alpha \leq 0.4 \text{ km}^{-1}$ ), the CNR at the 5-km range was higher than 7 dB even for the lowest volume backscatter coefficient ( $\beta = 3 \times 10^{-8} \text{ m}^{-1} \text{ sr}^{-1}$ ). Since  $\alpha$  is usually smaller than  $0.4 \text{ km}^{-1}$  for a clear atmosphere, we can properly conclude that the maximum range  $R_{\text{max}}$  of our lidar is 5 km. In mid-summer,  $\alpha$  sometimes exceeded  $0.4 \text{ km}^{-1}$ , which degraded  $R_{\text{max}}$ . The highest  $\alpha$  obtained from the meteorological measurement was  $\sim 0.7 \text{ km}^{-1}$ , which reduced  $R_{\text{max}}$  to  $\sim 3$  km. When the visibility was better than 3 km, the aerosol extinction was negligible, and the range capability of the lidar was not affected by it.

We estimated  $\beta$  using the coherent lidar at an altitude lower than  $\sim 30$  m where it will be in practical use. As the lidar receiver had been calibrated,  $\beta$  was derived from the measured CNR value using the following equation:

$$\beta = \text{MDP} \cdot \text{CNR} \frac{2R^2}{cE_t A_r} \exp(2\alpha R),$$

where  $E_t$  is the pulse energy and  $c$  is the light velocity.

Figure 5 shows a typical  $\beta$  distribution and a backscattered signal from which  $\beta$  was derived. Because the

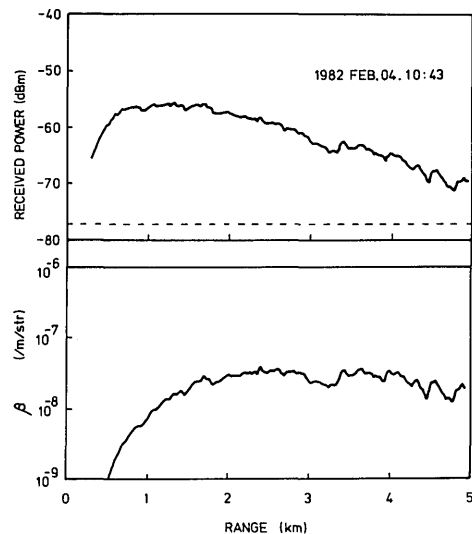


Fig. 5. Backscattered signal and derived  $\beta$  distribution;  $N = 30$ ,  $B_{\text{vid}} = 1.5$  MHz.

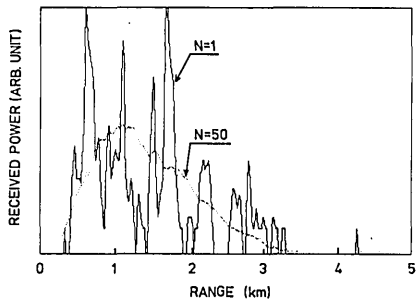


Fig. 6. Return signal waveforms;  $B_{\text{vid}} = 1.5$  MHz.

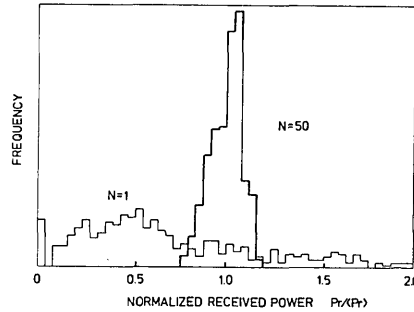


Fig. 7. Histogram of the normalized received power; for  $N = 1$ , IRRV is 1.8. By integrating fifty echoes, IRRV is improved to  $\sim 12$ .  $B_{\text{vid}} = 1.5$  MHz.

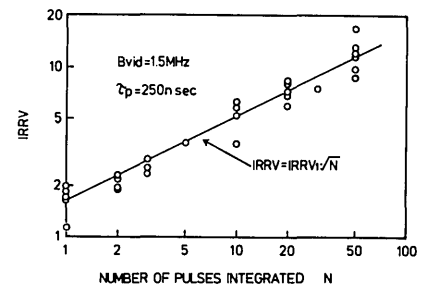


Fig. 8. IRRV improvement by integration;  $B_{\text{vid}} = 1.5$  MHz, PRF = 5 Hz.

field of view of the receiver and the section of the transmitted beam did not overlap completely at close range, the estimated  $\beta$  values are too small. So,  $\beta$  samples at ranges  $>2$  km were averaged to get  $\beta$  at that time. The results, ranging from  $3 \times 10^{-8}$  to  $8 \times 10^{-7} \text{ m}^{-1} \text{ sr}^{-1}$ , are consistent with data integrated by Post.<sup>12</sup>

#### D. Speckle Suppression and System Sensitivity

The system sensitivity to the target gas is dominated by the accuracy of the backscattered signal measurements. We measured IRRV of the received power and related it to the detection sensitivity.

The echo of a single pulse fluctuates greatly as shown by the solid curve in Fig. 6. The dotted curve shows a backscattered signal averaged by integrating fifty echoes. The strong fluctuation was reduced by interpulse averaging, and the accuracy of the measurement was improved as shown in Fig. 7, which shows that an IRRV of  $\sim 1.8$  for a single-pulse echo increases to 12 when fifty echoes are integrated.

The dependence of IRRV( $P_r$ ) on the number of pulses integrated,  $N$ , is shown in Fig. 8. The solid line represents the dependence predicted by Eq. (6). The figure shows that the backscatters from aerosols are not correlated with each other for a pulse rate of 5 pps. On an average, IRRV( $P_r$ ) is  $\sim 12$  for  $N = 50$ , which corresponds to  $2.8 \times 10^{-4} \text{ m}^{-1}$  for  $S$  for  $\Delta R = 300$  m according to Eq. (7). By curve fitting, the IRRV for the single-pulse echo, IRRV<sub>1</sub>, is determined to be 1.6 when  $B_{\text{vid}} = 1.5$  MHz. For  $B_{\text{vid}} = 0.55$  MHz, IRRV<sub>1</sub> was measured as 2.6. The results agree with the values obtained by using Eq. (5) from the system parameters, when we assume that  $B_I T$  in the equation can be estimated by  $(\tau_p B_{\text{vid}})^{-1}$  and that  $M = 1$ .

The system sensitivity to the target gas  $S$  was determined by carrying out RRDA measurement without target gas. Figure 9 shows a derived gas concentration profile. By averaging the values,  $S$  was estimated to be  $\sim 3.7 \times 10^{-4} \text{ m}^{-1}$  for  $\Delta R = 300$  m and  $7.4 \times 10^{-4} \text{ m}^{-1}$  for  $\Delta R = 150$  m when  $N = 50$  and PRF = 5 pps.

In Fig. 10, the measured values of  $S$  are compared with the values evaluated from IRRV<sub>1</sub> using Eq. (7), which are represented by the solid lines. For  $N$  smaller

than 30, the sensitivity is dominated by the residual speckle and agrees with the calculated value. For a larger  $N$ , the measured  $S$  departs from  $N^{-1/2}$  behavior while IRRV( $P_r$ ) is proportional to  $\sqrt{N}$  even for  $N > 30$ . And the scatter in  $S$  values for  $N = 50$  is larger than that in the corresponding IRRV values. This means that the additional error was caused by temporal changes in the light path condition which become significant during the time interval between the backscatter measurements for the two wavelengths. Figure 11 shows an extreme case where a large false indication appears at the 2.8-km range. At altitudes lower than 30 m, backscatter signals were subject to such irregularities, which were presumably attributed to backscatter from aerosols of urban origin and to extinction by pollutant gases or water vapor in stack plumes.

The RRDA technique in itself should have eliminated the errors caused by the irregularities in backscatter, but the measurement interval seems to have been too long. If the interval is sufficiently shortened, such additional errors can be reduced, as shown in Fig. 12. The return signal waveforms were obtained from two sets of fifty echoes which were measured successively; the interval was 10 sec. The waveforms agree with each other in spite of their strong irregularities, and  $S$  was not clearly degraded. In RRDA measurement, however, laser line selection and transmitter frequency control require a certain period of time, and it remains to be shortened. The simultaneous or alternating measurement of two frequency backscatters would be advantageous, although the lidar must have two transmitter lasers and LOs to do this.

#### E. Gas Detection Experiment

The range resolution of the system was determined by detecting a gas in a sample chamber. It could not be shown whether the measured values of  $C_0$  were consistent with the gas concentration in the chamber, because its windows were removed to avoid the extremely strong backscatter from them.

The chamber is a wooden box  $1.8 \times 0.9 \times 0.9$  m located  $\sim 1100$  m from the lidar. After assuring that the sidewall of the chamber did not scatter the transmitted laser pulse, target gas (Freon 12) was loaded into the

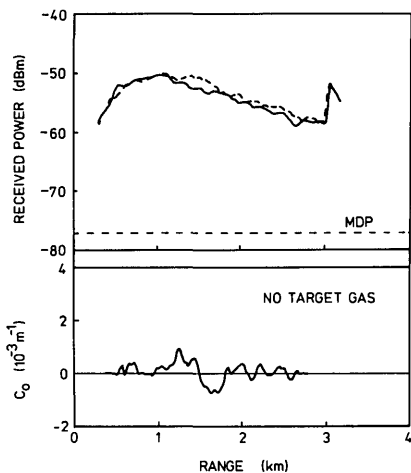


Fig. 9. Noise in a gas concentration profile;  $N = 50$ ,  $B_{\text{vid}} = 1.5$  MHz,  $\Delta R = 300$  m. The standard deviation of the noise or the sensitivity  $S$  is  $3.6 \times 10^{-4} \text{ m}^{-1}$ . The sharp peaks at 3 km are echoes returned from a roof which was in the field of view when the gas chamber was aimed at.

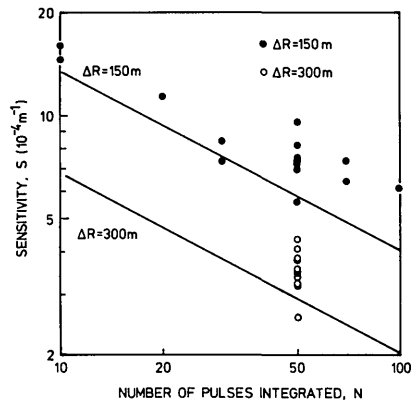


Fig. 10. Standard deviation of noise in the measured concentration or the sensitivity  $S$  vs the number of pulses integrated  $N$ ;  $B_{\text{vid}} = 1.5$  MHz, PRF = 5 Hz. Solid lines are  $S$  evaluated from  $\text{IRRV}_1$  using Eq. (6).

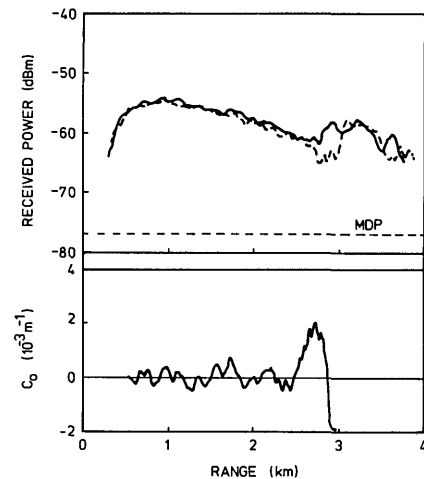


Fig. 11. False alarm caused by the backscatter irregularities;  $N = 50$ . The measurement interval was  $\sim 2$  min.

chamber. Then the echo signals were measured using  $10.6\text{-}\mu\text{m}$   $P(24)$  and  $P(34)$  lines and the RRDA reduction was performed to get the gas distribution profile. Figure 13 shows typical waveforms of echo signals and a reduced distribution profile, which definitely indicates the presence of the target gas. The system could locate the gas with accuracy; the range to the peak of the indication (1200 m) agrees with the range to the gas chamber. The range resolution or the full width at half-maximum concentration was 300 m, which agrees with the range interval  $\Delta R$  in RRDA reduction.

The hardware limit of the range resolution ( $\Delta R_m$ ), defined as the length of a range segment in which  $P_r$  decreases steeply due to the localized gas as shown in Fig. 13, was determined to be 200 m for  $B_{\text{vid}} = 1.5$  MHz, 270 m for 0.55 MHz. The range resolution was dominated by  $\Delta R$  as long as  $\Delta R$  was  $> \Delta R_m$ .

## V. Conclusion

The operation of a RRDA lidar with a heterodyne receiver has been demonstrated and its feasibility was experimentally confirmed. The maximum range was extended by employing heterodyne detection. In conditions of the usual extinction coefficient ( $\alpha \leq 0.4 \text{ km}^{-1}$ ), the system was capable of detecting signals backscattered at an  $\sim 5$ -km range with a CNR of  $\sim 7$  dB at least, which is enough to perform RRDA reduction. Even in the rather high extinction conditions ( $\alpha \approx 0.6 \text{ km}^{-1}$ ), the maximum range was  $\sim 3$  km.

Speckle fluctuation caused by the use of a highly coherent transmitting laser was reduced by integrating return signals to get enough  $\text{IRRV}(P_r)$ . With fifty integrations,  $\text{IRRV}(P_r)$  reached  $\sim 12$ , which corresponds to a sensitivity  $S$  of  $2.8 \times 10^{-4} \text{ m}^{-1}$  when the range resolution was set for 300 m. The experiment showed that fluctuation in the distribution of  $\alpha$  and  $\beta$  was another source of error in the derived gas concentration.

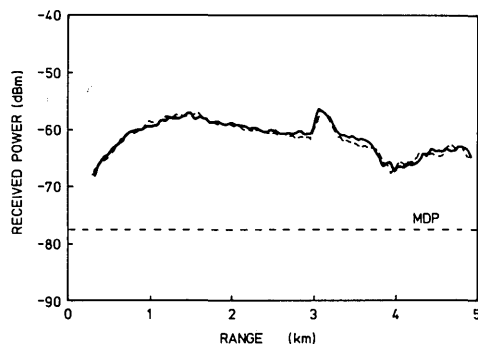


Fig. 12. Elimination of the  $\beta$  nonhomogeneity effect;  $N = 50$ . Without changing the laser line, 100 pulses were measured successively. The sensitivity  $S$  is estimated to be  $5.0 \times 10^{-4} \text{ m}^{-1}$ .

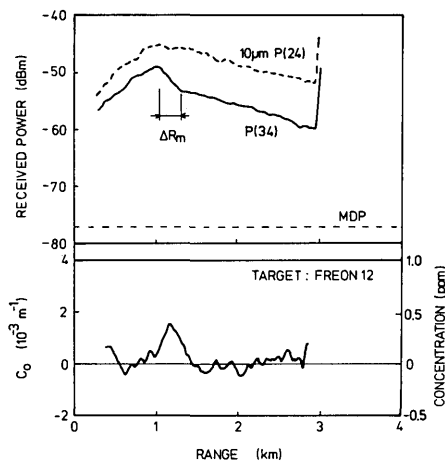


Fig. 13. Gas concentration profile. The range to the chamber is  $\sim 1100$  m.  $\Delta R = 300$  m,  $B_{\text{vid}} = 0.55$  MHz,  $N = 50$ ,  $\Delta k = 4.0 \times 10^{-3} \text{ ppm}^{-1} \text{ m}^{-1}$ .

Because of it,  $S$  derived from RRDA measurements increased to  $3.7 \times 10^{-4} \text{ m}^{-1}$  for  $\Delta R = 300 \text{ m}$ . If the interval between measurements for two wavelengths is shortened, detection sensitivity would improve. The range resolution of the system was limited to  $\sim 200 \text{ m}$ . Within this limit, the range resolution was dominated by  $\Delta R$  or  $B_{\text{vid}}$ .

From these results we have concluded that RRDA lidar with heterodyne detection is the most promising scheme for a long-range gas monitoring system.

The authors gratefully acknowledge the technical assistance provided by M. Tajima and H. Kashiwara.

## References

1. E. V. Browell, T. D. Wilkerson, and T. J. McIlrath, "Water Vapor Differential Absorption Lidar Development and Evaluation," *Appl. Opt.* **18**, 3474 (1979).
2. W. B. Grant, R. D. Hake, Jr., E. M. Liston, R. C. Robbins, and E. K. Proktor, Jr., "Calibrated Remote Measurement of  $\text{NO}_2$  using the Differential-Absorption Backscatter Technique," *Appl. Phys. Lett.* **24**, 550 (1974).
3. K. Asai, T. Itabe, and T. Igarashi, "Range-Resolved Measurements of Atmospheric Ozone using a Differential-Absorption  $\text{CO}_2$  Laser Radar," *Appl. Phys. Lett.* **35**, 60 (1979).
4. T. Kobayasi and H. Inaba, "Infrared Laser Radar Technique Heterodyne Detection for Range-Resolved Sensing of Air Pollutants," *Opt. Quantum Electron.* **7**, 319 (1975).
5. E. Jakeman, C. J. Oliver, and E. R. Pike, "Optical Homodyne Detection," *Adv. Phys.* **24**, 349 (1975).
6. P. Brockman, R. V. Hess, L. D. Staton, and C. H. Bair, "DIAL with Heterodyne Detection Including Speckle Noise: Aircraft/Shuttle Measurement of  $\text{O}_3$ ,  $\text{H}_2\text{O}$ , and  $\text{NH}_3$  with Pulse Tunable  $\text{CO}_2$  Lasers," NASA CP-2138, International Conference on Heterodyne Systems and Technology, Williamsburg, Va. (Mar. 1980).
7. R. M. Hardesty, "A Comparison of Heterodyne and Direct Detection  $\text{CO}_2$  DIAL Systems for Ground-Based Humidity Profiling," NOAA Technical Memorandum ERL WPL-64 (1980).
8. B. J. Rye, "Differential Absorption Lidar System Sensitivity with Heterodyne Reception," *Appl. Opt.* **17**, 3862 (1978).
9. J. H. Shapiro, B. A. Capron, and R. C. Harney, "Imaging and Target Detection with a Heterodyne-Reception Optical Radar," *Appl. Opt.* **20**, 3292 (1981).
10. M. Yoshikawa, T. Fukuda, and T. Akamatsu, "Wide Bandwidth HgCdTe Photodiode and Heterodyne Detection," in *Proceedings, First Sensor Symposium*, Tsukuba, Japan (June 1981), pp. 235-239.
11. R. A. McClatchey and A. P. D'Agati, "Atmospheric Transmission of Laser Radiation: Computer Code LASER," ERP 622, Air Force Geophysics Laboratory (Jan. 1978).
12. M. J. Post, in "Feasibility Study of Satellite-Borne Lidar Global Wind Monitoring System," R. M. Huffaker, Ed., NOAA Technical Memorandum ERL WPL-37 (1978).

## Seventh International Conference on Laser Spectroscopy (SEICOLS)

Maui, Hawaii, USA, June 24-28, 1985

The Seventh International Conference on Laser Spectroscopy will be held from June 24-28, 1985 at the Maui Surf Hotel, Maui, Hawaii. Among the topics to be discussed at this conference are fundamental physical application of laser spectroscopy, new laser spectroscopic techniques, novel applications of laser spectroscopy and new coherent light sources. For more information write to T. W. Hansch, Physics Department, Stanford University, Stanford, CA 94305, USA, or Y. R. Shen, Physics Department, University of California, Berkeley, CA 94729, USA.